

**Key Points:**

- Hydrometeorological impacts due to urban irrigation are examined based on WRF model simulations with a simple irrigation scheme
- The impacts of urban irrigation on surface heat fluxes and rainfall extend beyond local scales through perturbations to atmospheric forcings
- Accurate representations of human water consumption are important in characterizing land-atmosphere interactions in arid/semiarid regions

**Correspondence to:**

L. Yang,  
yanglong86123@hotmail.com

**Citation:**

Yang, Y., Smith, J., Yang, L., Baeck, M. L., & Ni, G. (2019). Regional impacts of urban irrigation on surface heat fluxes and rainfall in central Arizona. *Journal of Geophysical Research: Atmospheres*, 124, 6393–6410. <https://doi.org/10.1029/2018JD030213>

Received 23 DEC 2018

Accepted 23 MAY 2019

Accepted article online 10 JUN 2019

Published online 24 JUN 2019

## Regional Impacts of Urban Irrigation on Surface Heat Fluxes and Rainfall in Central Arizona

Yan Yang<sup>1,2</sup> , James Smith<sup>2</sup>, Long Yang<sup>3</sup> , Mary Lynn Baeck<sup>2</sup>, and Guangheng Ni<sup>1</sup>

<sup>1</sup>Department of Hydraulic Engineering, Tsinghua University, Beijing, China, <sup>2</sup>Department of Civil and Environmental Engineering, Princeton University, Princeton, NJ, USA, <sup>3</sup>School of Geography and Ocean Science, Nanjing University, Nanjing, China

**Abstract** Rapid urbanization over Phoenix has resulted in increased water consumption for maintenance of green spaces and heat stress mitigation. The hydrometeorological impact of urban irrigation is not well understood and is the principal objective of this study. Our results are based on high-resolution numerical experiments using the Weather Research and Forecasting model. A simple irrigation scheme is implemented into the Weather Research and Forecasting model to represent changes in soil moisture due to irrigation. A monthlong simulation using the Weather Research and Forecasting model with irrigation shows improved model performance in representing the regional water and energy cycle. Comparisons of model simulations with and without irrigation highlight the regional impacts of urban irrigation on surface heat fluxes and rainfall variability over Phoenix. There is a strong modulation of irrigation on surface energy partitioning over both irrigated and nonirrigated areas. Irrigation increases (decreases) surface latent (sensible) heat fluxes by enhanced evapotranspiration over irrigated areas, with opposing changes presented over nonirrigated areas. Irrigation contributes little to the domain-average rainfall accumulation, but can noticeably modify its spatial distribution, with increased rainfall over the downwind mountainous regions and decreased rainfall over the irrigated areas. Irrigation-induced rainfall anomalies can be tied to strengthened thermal gradients and induced changes in surface pressure fields, which lead to perturbations on large-scale flow and its interactions with complex terrain. Our results shed light on the hydrometeorological impacts of increasing anthropogenic water use driven by urbanization and highlight the importance of accurate representations of land surface processes in better characterizing land-atmosphere interactions in arid/semiarid regions.

### 1. Introduction

With more than half of metropolitan cities (population of more than 100,000) located in arid/semiarid regions, urban climate and other environmental issues related to urbanization have received particular attention in recent years. Rapid urban expansion places an increasing demand of irrigation for public green spaces (e.g., parks, grasslands), sporting grounds and private gardens (Mitchell et al., 2001; Richter, 2013; Vahmani & Hogue, 2014), and makes water-scarce conditions even more acute in arid/semiarid regions. Understanding and quantifying the impacts of urbanization and the increasing anthropogenic water use on regional climate are critical for better city designs and planning of urban complexes in arid/semiarid regions.

Our study region centers on the Phoenix, Arizona metropolitan region in the arid/semiarid southwestern United States. This region has witnessed rapid and extensive land use and land cover changes from agricultural and desert land into urban and suburban residential areas during the second half of the twentieth century (e.g., Chow et al., 2012; Georgescu et al., 2009a, 2009b; Hirt et al., 2008). Both observational and numerical modeling analyses have demonstrated significant influences of land use and land cover changes on the hydrological cycle and surface energy budget over Phoenix. We provide a brief summary of previous hydrometeorology studies concerning land use and land cover changes over Phoenix in Table 1.

Accompanied by rapid urbanization, the municipal outdoor water use for Phoenix is growing rapidly (Gober & Kirkwood, 2010), with more water demand for maintaining urban green space (including residential, commercial, and recreational districts) and mitigating thermal stress in the city during summer (e.g., Gober et al., 2009; Lemonsu et al., 2015; Yang & Wang, 2015). Based on the statistics of water consumption in 2015 for Maricopa County, Arizona, golf courses are estimated to consume 3,785 m<sup>3</sup> water per day for

**Table 1**  
*Summary of Previous Observational and Numerical Modeling Studies over Phoenix*

No.	Study period	Methods	Main findings	Reference
1	July to September of 1950–2000	Rain gauge observations	Increased rainfall downwind of Phoenix due to anthropogenic activities (urbanization and irrigation)	Diem and Brown (2003)
2	July of six years	Regional Atmospheric Modeling System	Contrasting roles of urbanization and irrigated cropland in temperature; increased rainfall due to urbanization	Georgescu et al. (2008)
3	July of six years	Regional Atmospheric Modeling System	Strong influence of land use and land cover changes on surface energy partitioning	Georgescu et al. (2009a)
4	July of six years	Regional Atmospheric Modeling System	Noticeable impacts of land use and land cover changes on convective activities	Georgescu et al. (2009b)
5	June of 2007	LUMPS	Irrigation can reduce nighttime temperature, with the effect depending on irrigation amount	Gober et al. (2009)
6	Four heat-wave events	WRF/UCM	Urbanization increase nighttime temperature by up to 10 K	Grossman-Clarke et al. (2010)
7	July of 1979, 1989, and 1994	WRF/UCM	Urbanization produce nighttime warming and daytime cooling over the city	Georgescu et al. (2011)
8	2006–2008	WRF/UCM	Mitigation of cool-roof on urban-induced warming	Georgescu et al. (2012)
9	2012	UCM	Urban irrigation cools the building environment by up to 3 K	Yang and Wang (2015)
10	July and August for 2005 and 2050	WRF/UCM	Urbanization in Phoenix-Tucson corridor is projected to increase air temperature, but reduce rainfall over the urban areas	Z. Yang et al. (2015)
11	2006	WRF/UCM	Green-roofs can reduce air temperature but increase humidity over urban areas	Yang et al. (2016)
12	January to September of 2015	Eddy covariance observations	Strong modulation of outdoor water use on surface heat fluxes	Templeton et al. (2018)
13	25 May to 31 August in 2012	WRF/UCM	Irrigated green roofs and white roofs both enhance probability of rainfall toward the outskirts of Phoenix	Song et al. (2018)

irrigation, additional water demand arises from intensive water use for public parks and surrounding croplands. In this study, we examine the regional impacts of urban irrigation on surface heat fluxes and space-time rainfall variability in central Arizona. We use the term urban irrigation to refer to all activities of outdoor water use within the city (e.g., irrigation for golf courses, grasslands, and private gardens), as well as irrigated croplands surrounding the urban core (see Figure 1 for details).

Urban irrigation is a critical component of the regional water cycle in arid/semiarid cities, which characterizes the so-called “oasis effect” phenomenon (Georgescu et al., 2011; Oke, 1979; Vahmani & Hogue, 2014, 2015). Enhanced evapotranspiration from increased soil moisture contributes substantially to latent heat flux in the surface energy budget. The outdoor water use modulates the partitioning of available energy between sensible and latent heat fluxes (Taylor et al., 2012; Templeton et al., 2018). Due to decreased sensible heat flux, urban-canyon air temperature can be more than 3 °C cooler, which helps to reduce thermal stress in the cities during summer (Yang & Wang, 2015). The reductions of daily maximum air temperature due to irrigation are evident over all urban land use types, with the low-intensity residential areas exhibiting the largest influence (Vahmani & Hogue, 2015). While most previous studies focus on the impacts of irrigation on hydrometeorological variables at local scales (see Table 1 for summary), we examine whether the hydrometeorological impacts of urban irrigation extend beyond local scales, and are evident at regional scales.

The impact of large-scale agricultural irrigation on rainfall has been extensively investigated and debated in previous studies (e.g., DeAngelis et al., 2010; Fowler et al., 2018; Im et al., 2014; Im & Eltahir, 2014; Mahalov et al., 2016; Zhang et al., 2017). Irrigation through increased soil moisture can possibly increase rainfall mainly due to enhanced low-level moisture availability and increased moist static energy for convection. On the other hand, irrigation can also make the atmosphere more stable through the evaporative cooling effect which inhibits rainfall. There is a large literature focusing on the feedback between soil moisture and rainfall (e.g., Alter et al., 2015; D’Odorico & Porporato, 2004; Eltahir, 1998; Findell et al., 2011; Guillod et al., 2015; Taylor et al., 2012; Welty & Zeng, 2018). The impacts of soil moisture on rainfall are not confined to the local scale (i.e., irrigated regions), they also show strong dependence on synoptic-scale atmospheric conditions (Findell & Eltahir, 2003; Fowler et al., 2018; Welty & Zeng, 2018). Im and Eltahir (2014) found that irrigation over West Africa increases rainfall in the upstream portion of the Niger River

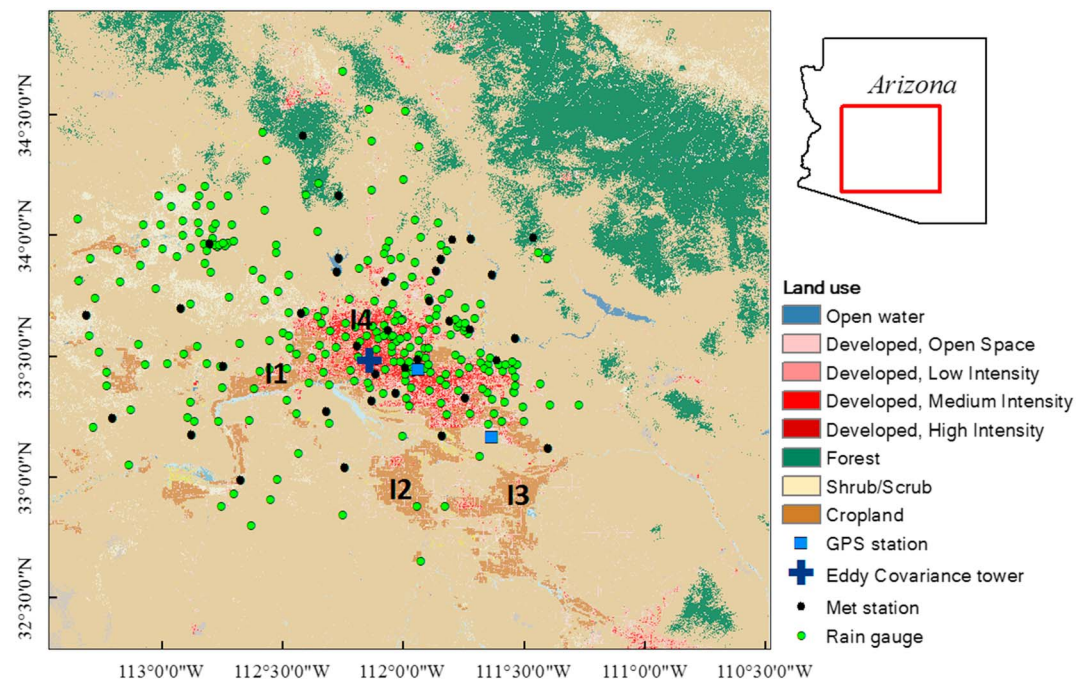


**Figure 1.** Map of study region. Scatters represent locations of meteorological stations, rain gauges, GPS stations, and eddy covariance tower, with the background as land use. I1, I2, I3, and I4 label the irrigated areas in the IRR simulation. The insert map in the top right corner show the location of the study region in the state of Arizona.

basin and produces more runoff downstream. The modified atmospheric circulation associated with large-scale irrigation can make rainfall anomalies even more complicated and unpredictable (Alter et al., 2015; Fowler et al., 2018; Mahalov et al., 2016). A distinct feature of urban irrigation from large-scale agricultural irrigation is that a considerable fraction of urban vegetation irrigation is presented as isolated patches, such as private gardens and roadside trees (e.g., J. Yang et al., 2015). The regional impacts of urban irrigation on spatiotemporal rainfall variability are relatively less studied.

The metropolitan Phoenix area receives more than half of annual rainfall during the North American Monsoon season (starting in late June and extending to September; e.g., Adams & Comrie, 1997; Douglas et al., 1993), with the rainfall variability mainly controlled by monsoon-related moisture surges (e.g., Maddox et al., 1995; Mejia et al., 2015; Seastrand et al., 2014). Interactions between synoptic-scale feature and complex terrain determine the frequency and intensity of convective activities in this region (Carleton, 1986; Mazon et al., 2016; Yang et al., 2017; Yang & Smith, 2018). In this study, we propose that urban irrigation plays an important role in characterizing spatial rainfall variability through modifications of atmospheric forcing and interactions with complex terrain in central Arizona. Monsoon-related moisture surge is a first-order control in determining the temporal rainfall variability over the entire region.

Based on long-term rain gauge records, Diem and Brown (2003) and Diem (2006) show observational evidence of spatial rainfall anomalies in central Arizona which can be attributed to increased urban coverage and irrigation. Our analyses are based on high-resolution (1 km) numerical simulations using the Weather Research and Forecasting (WRF) model. A simple irrigation scheme was developed and incorporated into the WRF model (see section 2.2 for details). The major themes of this study are (1) the impact of urban irrigation on surface heat fluxes at both local and regional scale, (2) the impact of urban irrigation on the spatial and temporal distributions of rainfall, and (3) application of an explicit irrigation scheme in atmospheric modeling to capture key features of land-atmosphere interactions in arid/semiarid regions. We shed light on the physical mechanisms associated with regional impacts of urban irrigation on surface heat fluxes and rainfall variability in central Arizona. Improved understanding of hydrometeorological responses to human activities can be of paramount importance in mitigating water-related vulnerabilities and climate risks in rapidly urbanizing regions, and also provide guidelines on sustainable development for arid/semiarid cities.

The paper is organized as follows. In section 2, we introduce the study region, observational data, model configurations, and experimental setup. In section 3, we first provide evaluation of model simulations through comparisons against in situ observations and then examine the irrigation impacts on surface heat fluxes and space-time rainfall variability over central Arizona. Summary and conclusions are provided in section 4.

## 2. Data and Methodology

### 2.1. Study Region and Data

Our study region centers on the Phoenix metropolitan region and covers a major part of central Arizona, principally Maricopa County. This region is characterized by complex topography and heterogeneous land use/land cover. Elevation ranges from 100 m to more than 2,500 m above sea level, including the Mogollon Rim and White Mountains that extend to the northwest and low-lying desert to the southwest of the city. The dominant land use/land cover includes shrubland, forest, grassland, urban, and cropland (Figure 1).

The Flood Control District of Maricopa County maintains a dense network of hydrometeorological stations. There are 298 rain gauges, 35 weather stations (providing 2-m temperature and 2-m specific humidity), two GPS stations, and one eddy covariance tower (see Figure 1 for locations). The rain gauges and weather stations are clustered over the Phoenix metropolitan region with relatively low density over the surrounding rural regions, especially to the southwest of the urban core and the high-elevation terrains to the northeast. Rainfall, 2-m temperature, and 2-m specific humidity are observed at 15-min time interval. We integrate 15-min observations to hourly scale for further analyses. Two GPS stations located in urban and cropland sites, respectively, provide continuous records of precipitable water (i.e., water vapor integrated vertically over the entire atmospheric column) at 30-min time interval. The eddy covariance tower is used to characterize surface heat fluxes over the Phoenix metropolitan region. The eddy covariance tower is located in a suburban residential area with its footprint mainly composed of heterogeneous urban land cover (including low-rise buildings, pavement, undeveloped surface cover; see, e.g., Chow et al., 2014; Templeton et al., 2018 for details). Observations of surface heat fluxes (i.e., sensible and latent heat flux) are also integrated to hourly scale for further analyses. There is a radiosonde station at Tucson, Arizona (approximately 120 km to the southeast of Phoenix). The sounding observations, made twice a day (i.e., 0000 UTC and 1200 UTC), are obtained from the University of Wyoming radiosonde archive (<http://weather.uwyo.edu/upperair/sounding.html>). In this study, we characterize vertical wind profiles and dynamics of moisture transport over central Arizona based on the sounding observations.

### 2.2. Model Configuration

The WRF model is a fully compressible, nonhydrostatic, mesoscale model (e.g., Skamarock et al., 2008). In this study, we use the Advanced Research version of WRF v3.6.1. Three one-way nested domains were developed in the model (as shown in Figure 2). The horizontal grids are  $199 \times 199$ ,  $255 \times 255$ , and  $240 \times 240$ , with horizontal grid spacing of 9, 3, and 1 km, respectively. The outer domain (D01) covers the major portion of southwestern United States, part of northern Mexico, the western Gulf of Mexico, the Gulf of California, and eastern Pacific, while the innermost domain (D03) centers over Phoenix metropolitan region and covers the entire Maricopa County. There are 30 vertical sigma layers (from the surface layer to 100 hPa) configured in the model. Time steps for the model domains are 30, 10, and 3.3 s, respectively. We use the North American Regional Reanalysis fields (see <http://www.emc.ncep.noaa.gov/mmb/rreanal/> for details) for initial and boundary conditions of the simulation. The spatial and temporal resolution of North American Regional Reanalysis is 32 km and 3 hr, respectively.

We use the 20-category MODIS data set (with spatial resolution of 1 km) to represent the land use and land cover in the model. There is only one urban category in the MODIS land use data set and the spatial coverage of cropland does not reflect the real condition of land use in the study region. We update the land use in the study region (only for the urban and cropland category) by incorporating the high-resolution (30 m) National Land Cover data set (see <http://www.mrlc.gov/nlcd2011.php> for more details). The National Land Cover data set has four urban land use categories: open space, low intensity, medium intensity, and high intensity (see Figure 1). Accurate representation of heterogeneous land surface properties plays an important role in capturing key features of the urban environment (e.g., Li et al., 2013). In this study, the Noah land surface model is used to simulate land-atmosphere fluxes of heat and moisture over the

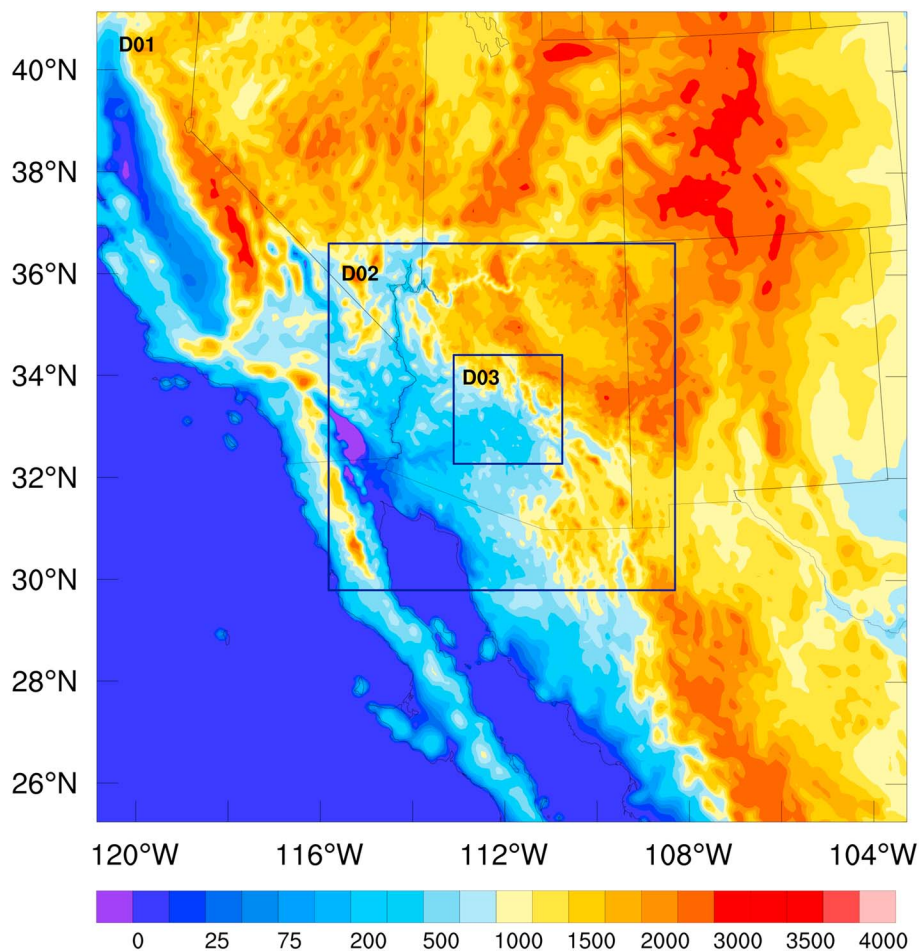


**Figure 2.** Configurations of model domains. Topography is shaded. The innermost domain (D03) is consistent with the red box shown in Figure 1.

nonurban grids. For urban grids, the single-layer Urban Canopy Model (see, e.g., Chen et al., 2011; Kusaka et al., 2001) is coupled to the Noah land surface model through a parameter of “urban fraction ( $\alpha$ ).” The Noah land surface model deals with the vegetated portion, while Urban Canopy Model calculates surface fluxes over urban surfaces. We use the default parameters for the single-layer Urban Canopy Model (see Chen et al., 2011, Table 1). The WRF single-layer Urban Canopy Model modeling system has been evaluated in previous studies with adequate ability in capturing daily evolution of surface variables (2-m temperature, wind, etc.; see, e.g., Salamanca et al., 2018). The physics options configured in the model are summarized in Table 2. The model configurations have been extensively evaluated in previous studies (especially refer to Yang and Smith (2018) for a simulation study of a severe convective monsoon storm over Phoenix). In this study, we further evaluate the capability of the modeling system in capturing key features of surface heat fluxes and dynamics of moisture transport at the monthly scale. Our model simulation starts from 0000 UTC 1 August 2014, and runs till 0000 UTC 31 August 2014. The output interval from the inner domain is 1 hr.

**Table 2**  
Summary of WRF Physics Options

Physics	Option
Microphysics	WSM 6
Boundary layer scheme	Yonsei University Scheme (YSU)
Longwave radiation	RRTM Scheme
Shortwave radiation	Dudhia Scheme
Surface layer	Monin-Obukhov Scheme
Cumulus parameterization	None
Surface urban physics	Single-layer UCM
Land surface	Noah land surface model
Land use	MODIS 20-category and NLCD 2011

### 2.3. Experiment Setup

We develop a simple irrigation scheme, and incorporate it into the WRF model to explicitly investigate the impacts of irrigation on surface heat fluxes and space-time rainfall variability over central Arizona. The

irrigation scheme is turned on only for model grids that belong to cropland categories (denoted as I1, I2, and I3 region in Figure 1) or urban land use categories (i.e., the low-intensity, medium-intensity, and high-intensity urban categories in National Land Cover data set, denoted as I4 region in Figure 1). There are 2,775 urban grids and 2,471 cropland grids in the innermost domain. For the urban grids, the irrigation scheme is only applied for the vegetated portion (determined by the urban fraction parameter  $\alpha$ ).

The basic idea of the irrigation scheme is to maintain soil moisture of the vegetated portion of urban and cropland grids at no less than field capacity. The irrigation scheme is applied for the full soil profile (four soil layers with a total thickness of 2 m) and takes the form

$$I_k = \begin{cases} 0, & \theta_{t,k} \geq \theta_f \\ (\theta_f - \theta_{t,k}) \cdot (1 - \alpha) \cdot d_k, & \theta_{t,k} < \theta_f \end{cases} \quad (1)$$

where  $I_k$  is the irrigation water amount (in meters) at soil layer  $k$  ( $k = 1, 2, 3, 4$ );  $\theta_f$  represents the field capacity ( $\text{m}^3/\text{m}^3$ ), while  $\theta_{t,k}$  represents the real-time volumetric soil moisture ( $\text{m}^3/\text{m}^3$ ) in time  $t$  at soil layer  $k$ ;  $d_k$  represents the thickness of soil layer  $k$  (i.e., 0.1, 0.3, 0.6, and 1.0 m for the four soil layers, respectively); and  $\alpha$  is the parameter of urban fraction (equals to 0.5 for low-intensity, 0.9 for medium-intensity, and 0.95 for high-intensity urban grids and equals to 0 for cropland grids). The field capacity varies with soil type and keeps constant over the entire soil profile.

We set up two contrasting simulations in this study. For the first simulation (referred to as “CTRL”), we turn off the irrigation scheme which allows the dynamics of soil moisture to be solely controlled by evapotranspiration and rainfall. During the dry-down period, soil moisture is quickly depleted due to strong potential evaporation rate in this region. For the second simulation (referred to as “IRR”), the irrigation scheme is applied at each individual time step for the cropland and urban grids. Both CTRL and IRR simulations use the same model configurations as previously described in section 2.2. The following analyses principally focus on the innermost domain for its high spatial resolution: analyses of moisture transport are conducted for domain 2 due to the location of the Tucson sounding station.

### 3. Results and Discussion

#### 3.1. Model Evaluation

We evaluate the performance of CTRL and IRR simulations through comparisons against surface observations (including 2-m temperature, 2-m specific humidity), precipitable water, and moisture transport by investigating their diurnal evolution together with their spatial and temporal distributions.

Figure 3 shows comparisons of composite diurnal cycles of 2-m temperature and 2-m specific humidity between observations from 35 weather stations and corresponding model grids from the two WRF simulations. The 2-m specific humidity exhibits a weak diurnal cycle and varies around 11.6 g/kg, while there is a strong diurnal cycle of 2-m temperature and peaks around 0000 UTC (1700 LST). Both CTRL and IRR simulations capture the key features of diurnal evolutions of near-surface air temperature and specific humidity.

The simulation results are statistically quantified via mean bias, root-mean-square errors, and correlation coefficient (see Table 3 for details). For the CTRL simulation, both 2-m air temperature and specific humidity are generally underestimated. There is a slight increase (decrease) in specific humidity (temperature) for the IRR simulation. The mean bias of specific humidity for the IRR simulation has been reduced to  $-0.57$  g/kg (compared to  $-0.71$  g/kg in the CTRL simulation). The alleviated dry biases are consistent with the underestimation of 2-m temperature, which is mainly associated with the evaporative cooling effect. The mean bias of 2-m temperature increases from  $-1.11$  °C in the CTRL simulation to  $-1.43$  °C in the IRR simulation. Underestimation biases of temperature and specific humidity are relatively larger over urban stations than rural stations. Underestimations of near-surface and surface skin temperature by WRF model over the Phoenix metropolitan area have also been reported in previous studies (e.g., Grossman-Clarke et al., 2010; Salamanca et al., 2018; Z. Yang et al., 2015). Underestimated surface temperatures might be partially attributed to the uncertainties within the urban canopy model (e.g., model parameters, rough estimates of anthropogenic heat) and needs further investigation. The temperature bias demonstrated in our study is of

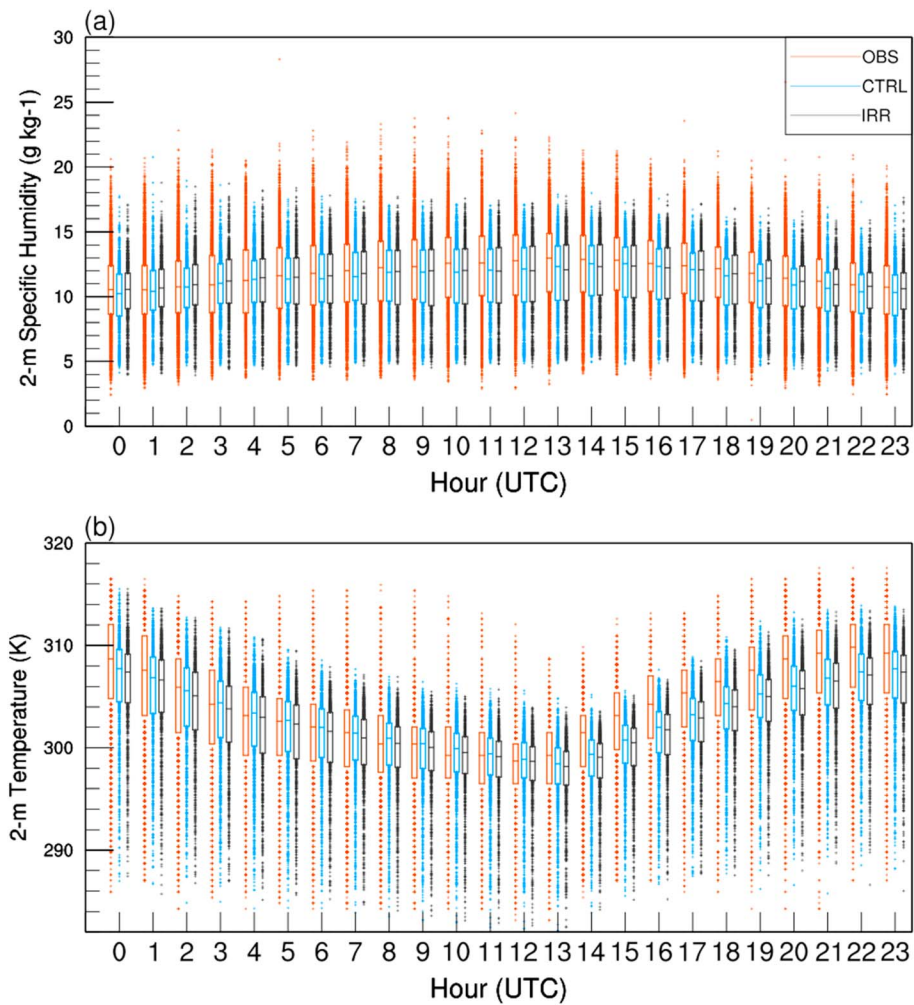


**Figure 3.** Monthly composite diurnal cycles of (a) 2-m specific humidity and (b) 2-m temperature during August 2014. The central mark on each box indicates the median, and the bottom (top) edge of each box indicates the 25th (75th) percentile. Outliers represent data beyond boxes from the minimum to the maximum which are marked with “cross” scatter. “OBS” (red) represents the observation data from 35 meteorological stations, while “CTRL” (blue) and “IRR” (black) represent the corresponding model grids containing the meteorological stations from CTRL and IRR simulation, respectively.

**Table 3**

*Evaluation Statistics for the CTRL and IRR (in Parentheses) Simulations Against Observations*

		Mean bias	Root-mean-square errors	Correlation coefficient
2-m specific humidity (g/kg)	All	-0.71 (-0.57)	2.45 (2.28)	0.71 (0.75)
	Urban	-1.11 (-0.86)	2.35 (2.18)	0.74 (0.78)
	Rural	-0.64 (-0.52)	2.47 (2.29)	0.70 (0.75)
2-m temperature (K)	All	-1.11 (-1.43)	3.08 (3.22)	0.81 (0.80)
	Urban	-1.20 (-1.98)	3.22 (3.62)	0.78 (0.77)
	Rural	-1.10 (-1.34)	3.05 (3.15)	0.81 (0.81)
Precipitable water (kg/m <sup>2</sup> )		2.32 (2.60)	5.77 (5.45)	0.84 (0.87)
IVT (kg m <sup>-1</sup> s <sup>-1</sup> )		92.1 (89.8)	136 (122)	0.61 (0.68)

*Note.* Statistics are averaged for all the stations or the corresponding model grids. The statistics are further classified into urban and rural stations according to their location.

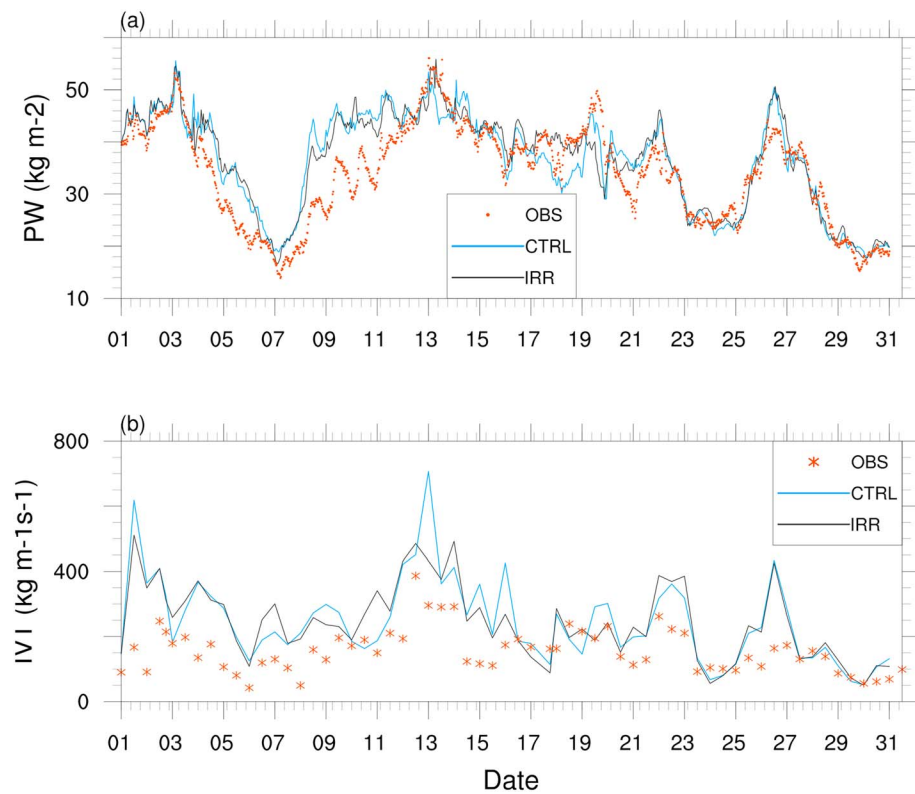


**Figure 4.** Monthly variations of (a) mean precipitable water vapor (PW) and (b) integrated water vapor flux (IVT). The dots (red) represent observation from GPS stations (a) and the radiosonde station (b), while the blue and black lines represent corresponding model grids from the CTRL and IRR simulation. The simulation results of IVT are from domain 2.

comparable magnitudes to previous studies (for instance, the cool bias are  $-0.91^{\circ}\text{C}$  and  $-1.11^{\circ}\text{C}$  in Z. Yang et al. (2015) and the CTRL simulation, respectively). The IRR simulation further intensifies the underestimation in 2-m temperature as expected (e.g., Eltahir, 1998; Gober et al., 2009; Grossman-Clarke et al., 2010). However, this does not imply worse model performance after incorporating the irrigation

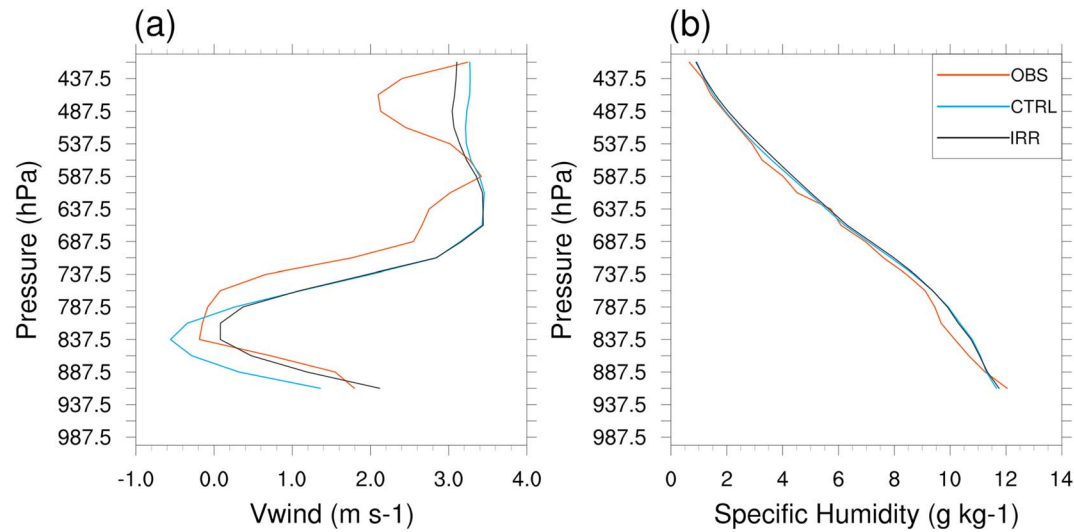


**Figure 5.** Vertical profiles of monthly mean (a) meridional wind speed (in m/s;  $v$  component) and (b) specific humidity (in g/kg) at 1200 UTC. The red lines indicate observations at the radiosonde station, and blue and black lines represent simulation results from the model grid that contains the radiosonde station in the CTRL and IRR simulation, respectively.

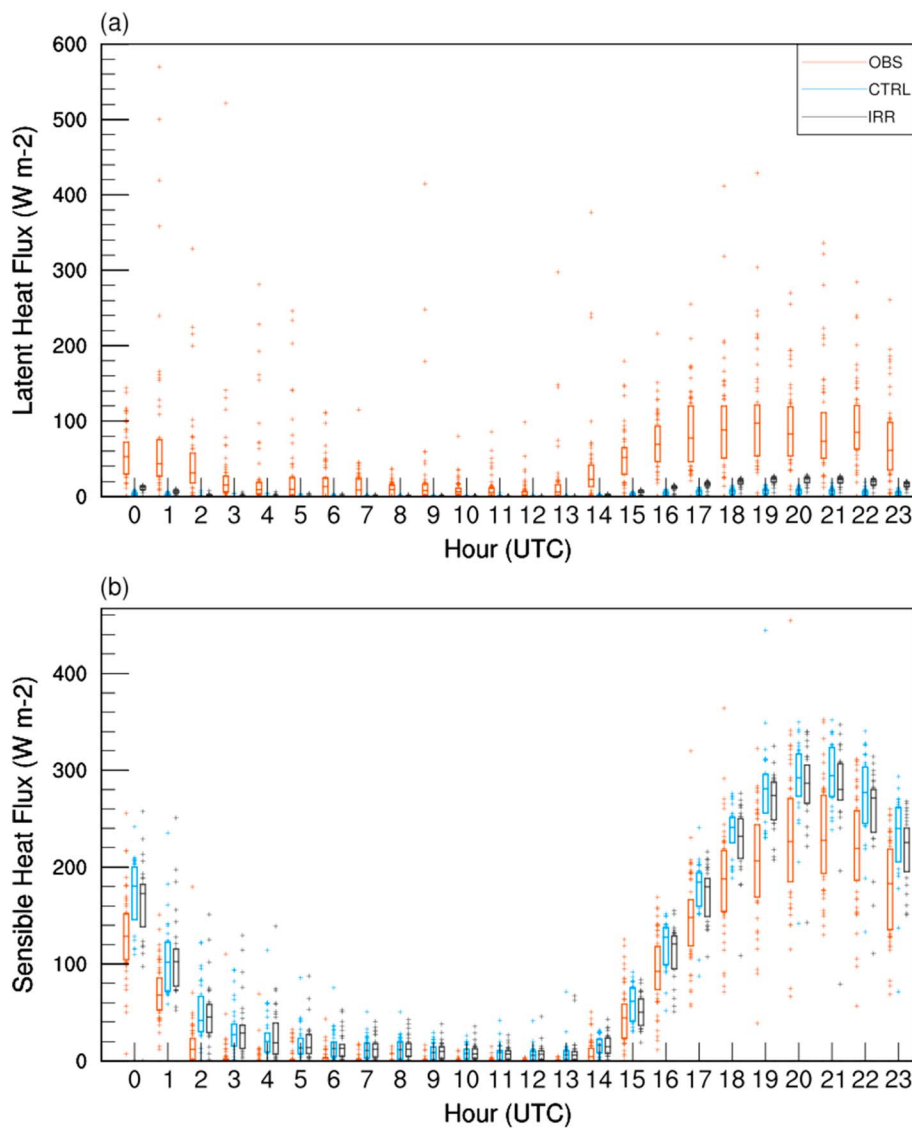


**Figure 6.** Box plots of diurnal cycles of (a) latent heat flux and (b) sensible heat flux during August 2014 from eddy covariance observation (red), CTRL simulation (blue), and IRR simulation (black) of the corresponding model grid containing the eddy covariance tower.

scheme. We will show below the WRF model with irrigation scheme greatly improve simulation of other hydrometeorological variables that regulate the water and energy cycles in Phoenix.

Figure 4a shows the temporal variations of mean precipitable water from the two GPS stations and the corresponding model grids from the CTRL and IRR simulations. The correlation coefficient (root-mean-square error) for CTRL and IRR simulations are 0.84 (5.77) and 0.87 (5.45), respectively, indicating good characterization of the timing and magnitude of monthly fluctuations in precipitable water during the simulation period. The temporal variations of precipitable water are closely tied to moisture transport, as indicated by the vertically integrated horizontal water vapor transport (IVT; integrated from the surface layer to around 400 hPa) from the Tucson sounding (Figure 4b). Both CTRL and IRR simulations capture synoptic-scale moisture transport, with slightly better performance shown for the IRR simulation. A common feature for both simulations is the general overestimation in the magnitudes of IVT. The overestimation can be attributed to the large meridional wind speed at the middle atmospheric layers (around 700–600 hPa; Figure 5a). The vertical profiles of specific humidity show consistency between the two model simulations and observations (Figure 5b). There are five storm episodes over central Arizona during August of 2014. The timings of

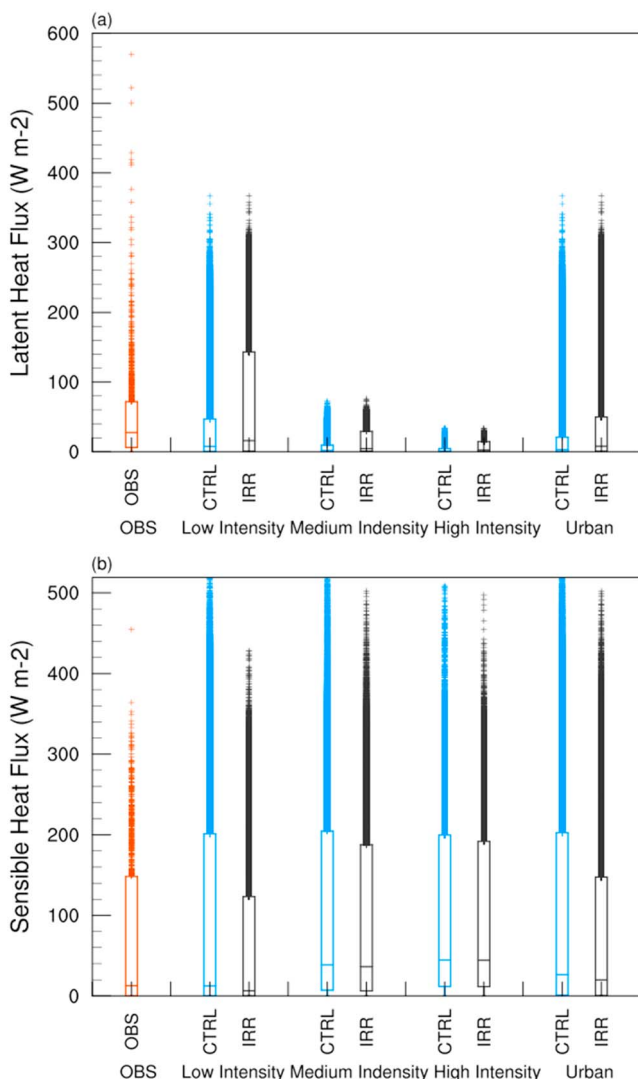


**Figure 7.** Box plots of monthly composite (a) latent heat fluxes and (b) sensible heat fluxes during August 2014 over different urban land use categories (low intensity, medium intensity, and high intensity). The first column represents observations from the eddy covariance tower. The last two columns of the box plots show the average over all three urban land use categories.

observational footprint. The eddy covariance tower is located in a heterogeneous urban setting with its footprint consisting of diverse land surfaces. While in the model, the simulated surface heat fluxes of the model grid that contains the eddy covariance tower only represent characteristics of the high-intensity developed urban land surface. Thus, we further examine simulated surface heat fluxes over all types of urban grids (i.e., low intensity, medium intensity, and high intensity) surrounding the eddy covariance tower. The responses of surface heat flux to irrigation are highly sensitive to the vegetated portions of different land use types. As can be seen from Figure 7, the low-intensity developed urban grids show the largest variations of surface heat fluxes. The magnitudes of mean latent and sensible heat fluxes for all urban grids are 46 and 75 W/m<sup>2</sup>, respectively for the IRR simulation, which are comparable to the mean observed values of 53 and 71 W/m<sup>2</sup> from the eddy covariance station. The contrast of surface heat fluxes between CTRL and IRR simulations highlights the importance of accurate representations of land surface properties in characterizing surface energy budget in arid/semiarid urban environment.

the storm episodes are consistent with the bursts of IVT and precipitable water (figure not shown). The consistency of temporal variations of moisture transport and domain-averaged rainfall highlights the dominant role of moisture surge in characterizing the water cycle in arid/semiarid southwestern United States during the North American Monsoon period.

In general, the two simulations capture the key features of diurnal evolution of near-surface metrological variables and monthly dynamics of moisture transport over central Arizona. Biases in near-surface temperature in both CTRL and IRR simulations are within reasonable range, with slightly larger underestimation in the IRR simulation due to the expected evaporative cooling effect associated with the irrigation scheme. Significant improvements on hydrometeorological variables (e.g., near-surface specific humidity and moisture transport) demonstrate the utility of the irrigation scheme in simulating water and energy cycles in arid/semiarid southwestern United States.

### 3.2. Impacts of Irrigation on Surface Heat Fluxes

Diurnal cycles of surface heat fluxes (i.e., latent and sensible heat fluxes) from the eddy covariance station and the corresponding model grid in CTRL and IRR simulations are compared in Figure 6. Both simulations capture the diurnal variability of surface heat fluxes, but exhibit considerable bias, especially for latent heat flux (Figure 6a). The maximum median of the observed latent heat fluxes is around 100 W/m<sup>2</sup>, while the maximum latent heat fluxes from both simulations are less than 20 W/m<sup>2</sup>. Both simulations overestimate sensible heat fluxes at the model grid containing the eddy covariance station. We note that the IRR simulation shows improved results compared to the CTRL simulation in both latent and sensible heat fluxes (Figure 6). The mean biases of daytime mean latent heat flux and sensible heat flux are around -73 and 45 W/m<sup>2</sup>, respectively, for the CTRL simulation, while irrigation increases (decreases) the daytime mean latent (sensible) heat flux by 9 W/m<sup>2</sup> (8 W/m<sup>2</sup>) in the IRR simulation.

The simulated biases in surface heat fluxes can be partially attributed to representations of heterogeneous urban surfaces in the model. Surface energy budget over urban area is controlled by land surface characteristics, such as land cover types (urban fraction) and sky-view factor (Chow et al., 2014; Oke, 2006; Templeton et al., 2018). These properties are important in determining the spatial-temporal distributions of surface heat fluxes. A key assumption of the eddy covariance technique in urban setting is the homogeneity of land surface characteristics within the observational footprint. The eddy covariance tower is located in a heterogeneous urban setting with its footprint consisting of diverse land surfaces. While in the model, the simulated surface heat fluxes of the model grid that contains the eddy covariance tower only represent characteristics of the high-intensity developed urban land surface. Thus, we further examine simulated surface heat fluxes over all types of urban grids (i.e., low intensity, medium intensity, and high intensity) surrounding the eddy covariance tower. The responses of surface heat flux to irrigation are highly sensitive to the vegetated portions of different land use types. As can be seen from Figure 7, the low-intensity developed urban grids show the largest variations of surface heat fluxes. The magnitudes of mean latent and sensible heat fluxes for all urban grids are 46 and 75 W/m<sup>2</sup>, respectively for the IRR simulation, which are comparable to the mean observed values of 53 and 71 W/m<sup>2</sup> from the eddy covariance station. The contrast of surface heat fluxes between CTRL and IRR simulations highlights the importance of accurate representations of land surface properties in characterizing surface energy budget in arid/semiarid urban environment.

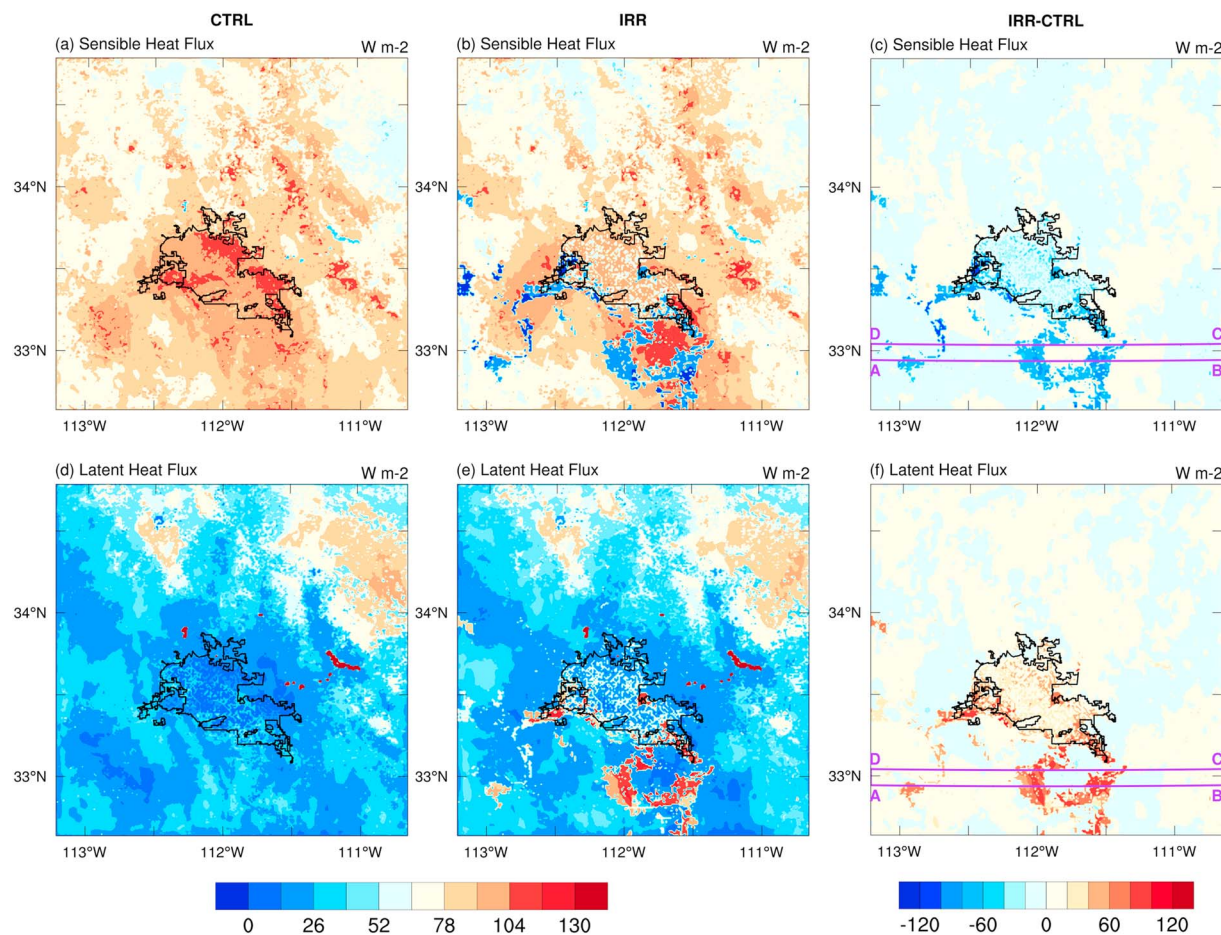


**Figure 8.** Spatial distribution of monthly average surface (a–c) sensible and (d–f) latent fluxes from (a and d) CTRL simulation, (b and e) IRR simulation, and (c and f) differences between two simulations (i.e., IRR minus CTRL). Figures 9a–9c and 9d–9f represent the sensible heat fluxes and the latent heat fluxes, respectively. Line AB and DC (purple) in (c) and (f) envelopes the area where longitudinal profiles (see Figures 9 and 10) are taken. The black contours show the city boundary of Phoenix.

Figure 8 shows spatial distributions of monthly mean sensible and latent heat fluxes from both simulations, as well as their differences. Due to elevated soil moisture from irrigation, the IRR simulation increases (decreases) latent (sensible) heat flux by 5 W/m<sup>2</sup> averaged over the entire domain, with the major contrasts presented over the irrigated areas. There are, however, some “anomalous” changes over nonirrigated regions surrounding the irrigated croplands, with increased sensible heat fluxes and decreased latent heat fluxes (Figures 8b and 8e), which exhibits opposite changes to those over the irrigated croplands. We construct longitudinal profiles between AB and DC that cross the “anomalous” region (as shown in Figure 8c), to further highlight the contrasting changes in surface heat fluxes over irrigated and nonirrigated areas. The averaged longitudinal profiles of daytime and nighttime surface heat flux differences between two simulations are shown in Figure 9. The dominant land uses over the enveloped region ABCD are cropland and shrubland. The irrigated croplands (I1, I2, and I3) show increased (decreased) latent (sensible) heat fluxes during the daytime. By contrast, the nonirrigated shrubland shows two distinctive patterns: the region enveloped by I2 and I3 show opposite changes to the cropland, while areas that are remote from irrigated croplands (i.e., to the left of I1 in the longitudinal profile) show similar changes to croplands. The differences between two simulations are consistent throughout the daytime and nighttime, with daytime exhibiting considerably large variations, indicating strong contribution of daytime evaporation to surface energy budget.

The anomalous region of surface sensible heat fluxes is associated with changes in temperature gradients. Figure 10 shows the averaged differences of longitudinal profiles of the surface skin temperatures, 2-m temperature, together with their differences. The IRR simulation produces higher surface skin temperature but

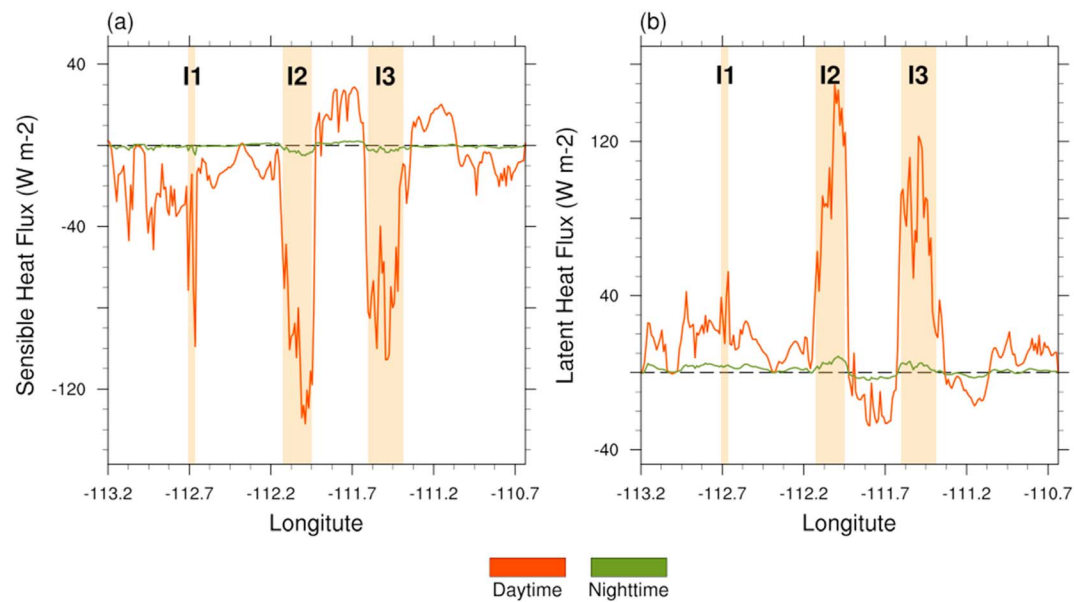


**Figure 9.** Mean longitudinal profiles of (a) sensible heat fluxes and (b) latent heat fluxes differences between IRR and CTRL simulations (i.e., IRR minus CTRL). Red and green lines represent averages for daytime (0800–2000 LST) and nighttime (2000–0800 LST), respectively.

lower 2-m temperature over the nonirrigated area between I2 and I3. The difference between surface skin temperature and 2-m temperature leads to the anomalous increase of sensible heat fluxes as shown in Figure 9a. The anomalous changes (i.e., decreases) of latent heat fluxes over nonirrigated areas (Figure 9b) are tied to the changes of rainfall, as will be detailed in the following section. The impact of irrigation on surface heat fluxes is not confined within the irrigated regions, but can extend beyond to regions that are in the vicinity of cropland.

The responses of surface heat fluxes to irrigation contrast in both the magnitude and the spatial variations. Elevated soil moisture induced by irrigation increases (decreases) latent (sensible) heat fluxes over the irrigated areas, but produces an opposite pattern over surrounding nonirrigated areas through exchanges of heat and moisture across regions. The WRF simulation with irrigation can reasonably capture the magnitude of surface heat fluxes over the Phoenix metropolitan region. Accurate representations of land surface processes play a critical role in characterizing surface energy budget in arid/semiarid urban environment.

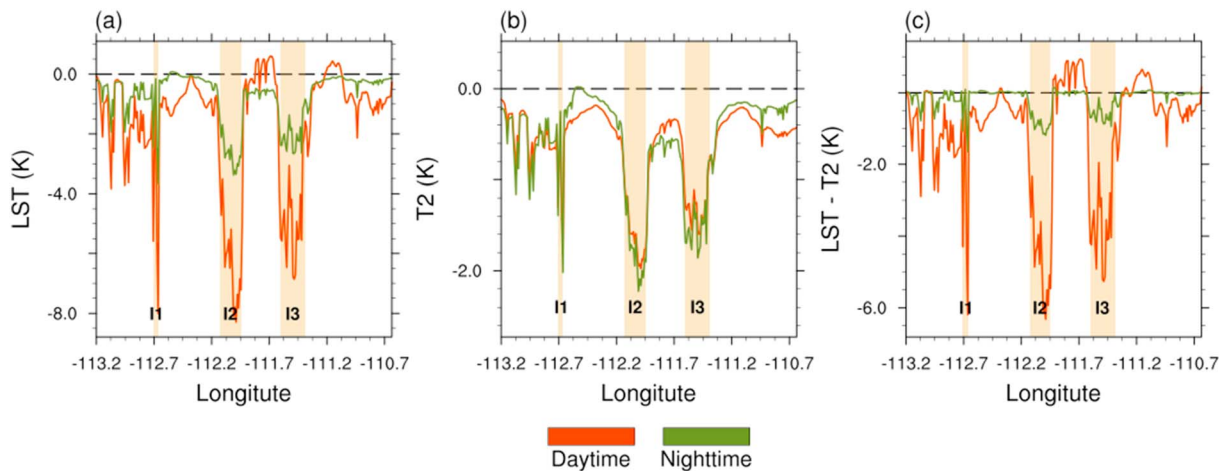


**Figure 10.** Same as in Figure 9 but for (a) surface skin temperature and (b) 2-m temperature differences between IRR and CTRL simulations (i.e., IRR minus CTRL) and (c) differences between (a) and (b).

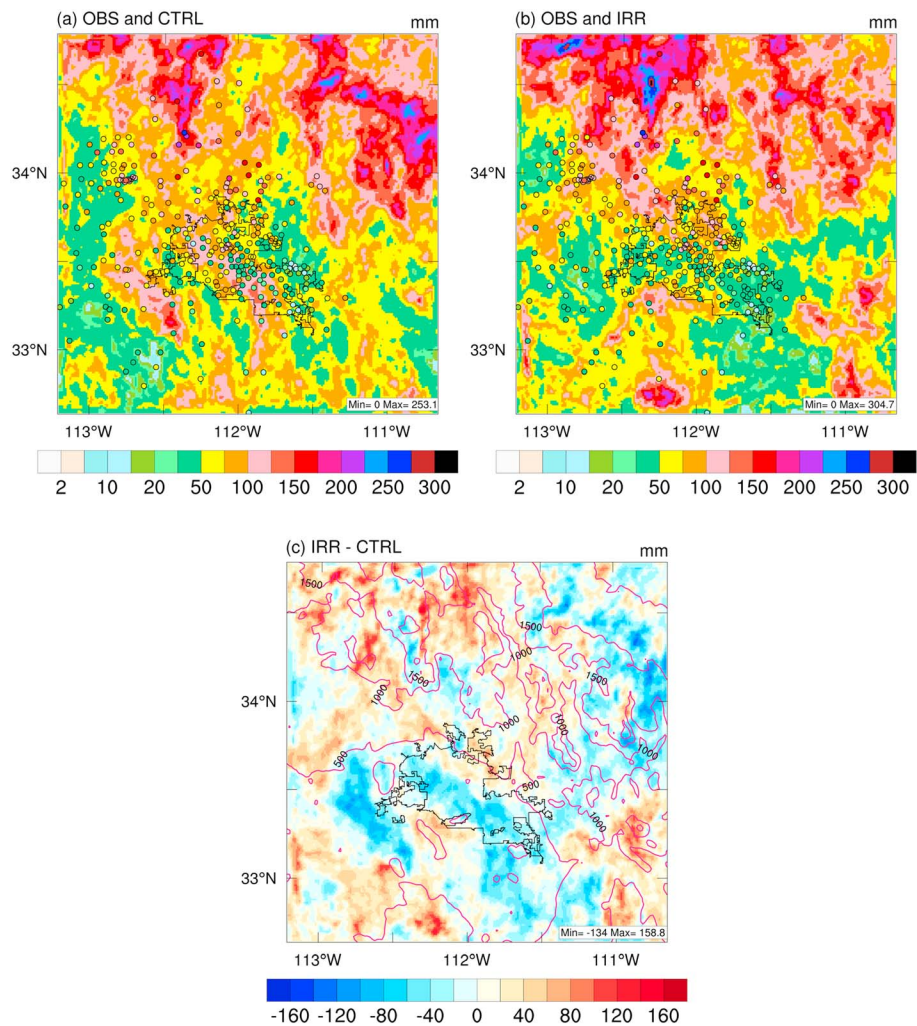


**Figure 11.** Spatial distributions of monthly rainfall accumulations (shade) from (a) CTRL and (b) IRR simulation and (c) their differences (i.e., IRR minus CTRL). The scatters in (a) and (b) indicate observed monthly accumulated rainfall from rain gauges. Pink contours in (c) represent topography with an interval of 500 m.

### 3.3. Impact of Irrigation on Rainfall

Figure 11 compares the spatial distributions of monthly rainfall accumulations between rain gauge observations and model simulations (i.e., CTRL and IRR). The monthly rainfall accumulations are 66 mm averaged over all the rain gauges, and are 70 and 68 mm averaged among the corresponding model grids for the CTRL and IRR simulation, respectively. The correlation coefficient increases to 0.5 in the IRR simulation compared to 0.25 for the CTRL simulation. There are 43 (24) rain gauges that show comparable rainfall accumulations (within 1 standard deviation) in the IRR (CTRL) simulation over the co-located model grids. A notable feature is the consistency of rainfall accumulations within the urban core region between the IRR simulation and gauge observations (Figure 11b), while the CTRL simulation shows significant overestimation (Figure 11a). There are contrasting spatial patterns of rainfall accumulations between the two simulations (Figure 11c). Compared to the CTRL simulation, there is a significant decrease of total rainfall over the irrigated regions (including the urban and cropland), but increased rainfall over the downwind mountainous regions (Figure 11c). Decreased rainfall over the surrounding nonirrigated area leads to reduced latent heat fluxes (between I2 and I3, as shown in Figures 9 and 10) due to limited soil moisture for evapotranspiration.

Figure 12 shows the spatial differences of 2-m specific humidity and 2-m temperature between the IRR and CTRL simulations (IRR minus CTRL). In general, the IRR simulation provides a wetter and cooler

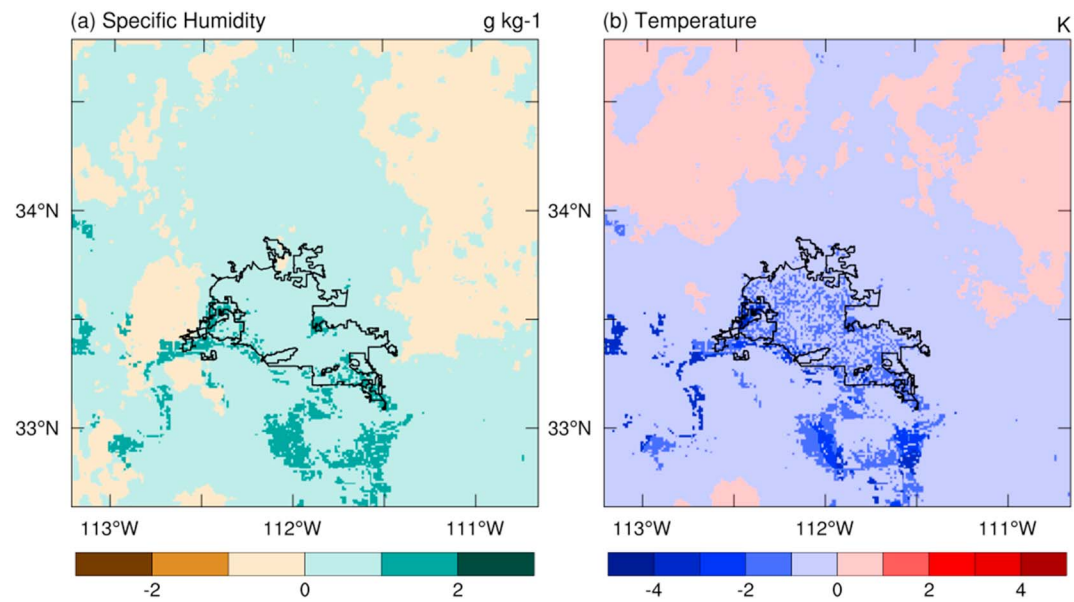


**Figure 12.** Spatial distributions of model difference (i.e., IRR minus CTRL) for monthly average (a) 2-m specific humidity (in  $\text{g/kg}$ ) and (b) 2-m temperature (in K).

environment than the CTRL simulation, which is consistent with the station-based analyses as shown in section 3.1. The differences averaged over the entire domain are  $0.15 \text{ g/kg}$  and  $-0.26 \text{ K}$  for 2-m specific humidity and temperature, respectively. Consistent with surface fluxes shown in section 3.2, the most notable differences of near-surface meteorological variables are confined within the irrigated regions, with only slight changes in the downwind mountainous regions.

To further understand spatial variations of rainfall accumulations induced by irrigation, we investigate the storm environment through comparisons of maximum convective available potential energy (CAPE) and maximum convective inhibition (CIN) between the IRR and CTRL simulations. Contrary to the spatial differences of near-surface meteorological variables or surface fluxes, differences of CAPE and CIN induced by

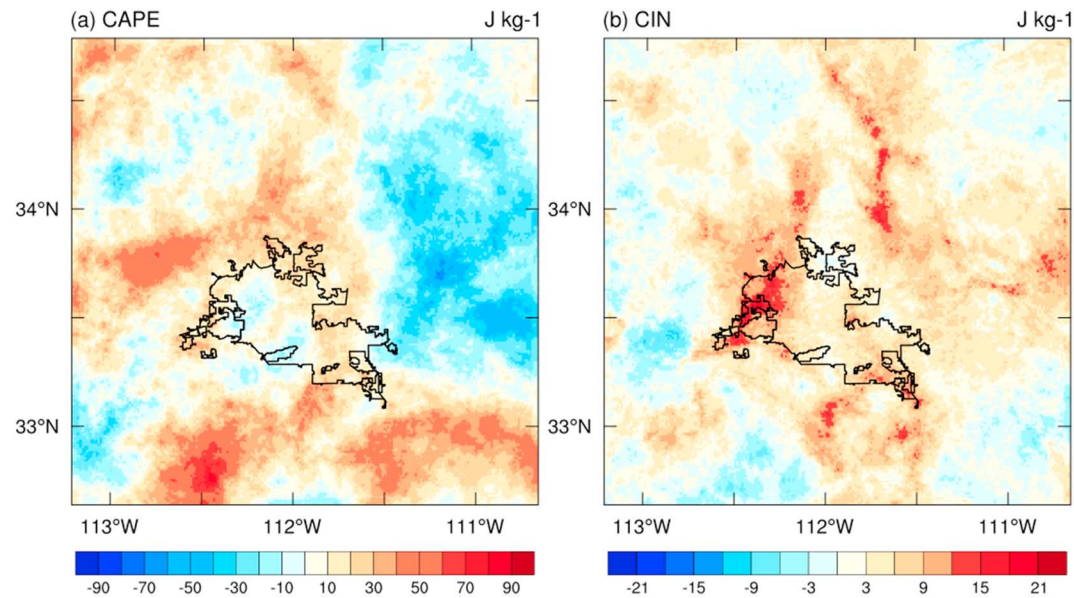


**Figure 13.** Spatial distributions of the model differences (i.e., IRR minus CTRL) for monthly average (a) maximum convective available potential energy (CAPE; in  $\text{J/kg}$ ) and (b) maximum convective inhibition (CIN; in  $\text{J/kg}$ ).

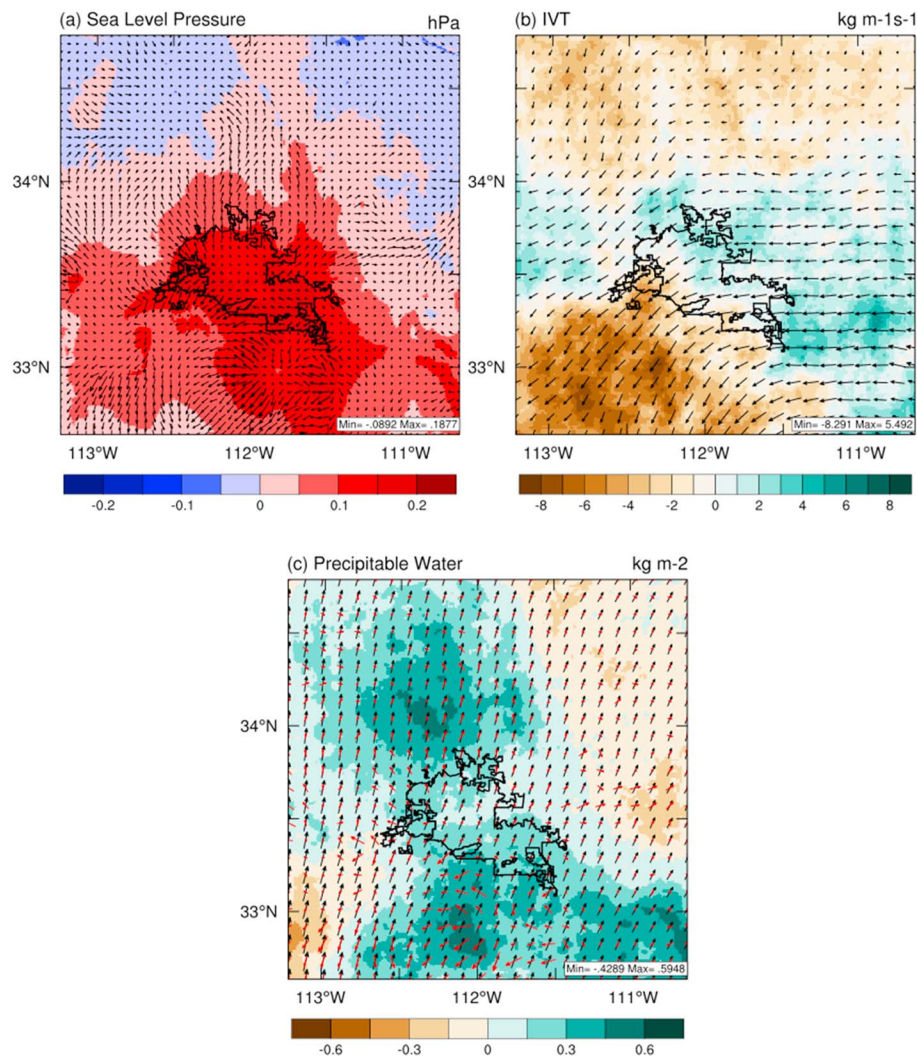


**Figure 14.** Spatial distribution of model differences (IRR minus CTRL) for monthly average (a) sea level pressure (in hPa), (b) integrated water vapor transport (IVT; in  $\text{kg m}^{-1} \text{s}^{-1}$ ) and (c) precipitable water (in mm). The black vectors overlaid (a)–(c) indicate 10-m wind and IVT differences between IRR and CTRL simulations and IVT of IRR simulation, respectively. Red vectors in (c) represent differences of 10-m wind fields between IRR and CTRL simulations.

irrigation can be identified at both local and regional scales (Figure 13). Increased CIN provides a more stable environment over irrigated areas that lead to decreased rainfall in the IRR simulation as a result of the elevated soil moisture and cooling effect of evaporation. Increased CAPE plays a more important role in increasing total rainfall over the downwind mountainous regions. Song et al. (2018) found enhanced probability of rainfall over the outskirts of Phoenix due to replacement of conventional roof with irrigated green roof over the city.

Rainfall increases in high-terrain regions can also be tied to the changing patterns of atmospheric forcing that are favorable for orographic enhancement of rainfall. Figure 14 shows the spatial differences of sea level pressure and low-level wind fields between the IRR and CTRL simulations. There is a high-pressure anomaly and induced low-level divergence over the irrigated area. The divergence is strongest near the boundary of irrigated and nonirrigated areas. There is strong convergence in the downwind mountainous region, together with enhanced atmospheric moisture content which directly contributes to elevated CAPE and rainfall.

The impact of irrigation on rainfall is not confined to the irrigated areas, but can extend to regional scales. There are only slight changes in total rainfall amount over the entire study region (D03). Contrasting

spatial distributions of the rainfall accumulation are closely tied to elevated soil moisture over irrigated areas, as well as the induced changes in thermodynamic fields and synoptic flows. The interactions of “perturbed” large-scale flow with mountainous terrain play a critical role in determining the spatial and temporal variability of rainfall, especially over the downwind region of the irrigated areas.

#### 4. Summary and Conclusions

In this study, we examine the regional impacts of irrigation on surface heat fluxes and space-time rainfall variability in central Arizona. We focus on a one-month period, August 2014, during the North American Monsoon season. Our results are based on high-resolution numerical experiments using the WRF model coupled with single layer Urban Canopy Model, together with empirical analyses of in situ observations from a dense network of meteorological stations over Phoenix, Arizona. A simple irrigation scheme is incorporated into the WRF single-layer Urban Canopy Model modeling system to accurately represent thermodynamic and dynamic perturbations of human water use on regional climate in an arid/semiarid urban environment. Major findings are summarized below.

1. The CTRL simulation (WRF “without irrigation”) captures general features of the regional water and energy cycles during the simulation period of August 2014, including day-to-day variability and composite monthly features of the diurnal cycle. The representations of near-surface temperature and humidity, as well as surface heat fluxes, in the CTRL simulation, however, have significant biases, compared to in situ observations. The IRR simulation (WRF with irrigation scheme) largely reduces the biases in 2-m specific humidity, IVT, surface heat fluxes, and accumulated rainfall, even though bias in 2-m temperature slightly increases due to the evaporative cooling effect after adding irrigation.
2. Latent heat flux from the CTRL simulation is underestimated in urban areas by  $20 \text{ W/m}^2$  on average. In the IRR simulation, the latent heat flux is increased to  $46 \text{ W/m}^2$  averaged over all irrigated urban pixels, which is comparable to observations ( $53 \text{ W/m}^2$ ) from an eddy covariance tower located in a heterogeneous urban region. For the nonirrigated areas, the changes of surface heat fluxes are related to the hotter and drier environment caused by decreased rainfall and soil moisture. These results are in line with previous observational analyses showing that irrigation plays an important role in surface energy partitioning in arid/semiarid urban environments (e.g., Templeton et al., 2018).
3. Both the CTRL and IRR simulations produce comparable rainfall accumulations over the entire study region and have similar temporal distributions of rainfall during the entire simulation period. The IRR simulation, however, captures the spatial distribution of rainfall in a way that is more consistent with observations. The negligible differences in rainfall timing and total amount between the two simulations indicate the first-order control of large-scale moisture transport in determining rainfall climatology in the southwestern United States during the North American Monsoon period.
4. There is a decrease of rainfall over irrigated areas in the IRR simulation, but an increase over the downwind mountainous region. The decrease in rainfall over irrigated regions is linked to increased atmospheric stability associated with the increased convective inhibition. Advection of moisture and interactions with prevailing large-scale flow result in increases in rainfall over complex terrain. The impacts of irrigation are not confined within irrigated regions, but can extend to regional scales through perturbations to atmospheric forcing.

While the majority of previous studies focus on land use/land cover changes, we highlight the importance of properly representing land surface processes in improved understanding of hydrometeorological impacts due to anthropogenic water consumption (e.g., irrigation for cropland, urban outdoor water use). Despite the simplicity of the irrigation scheme adopted in this study, we highlight the sensitivity of hydrometeorological fields to irrigation in an arid/semiarid urban environment. The impacts of irrigation on surface energy partitioning and rainfall spatial distribution highlight the importance of accurate representations of land surface processes in characterizing land-atmosphere interactions in an arid/semiarid urban environment. Future efforts will be dedicated to developing irrigation schemes with better representations of irrigation practices that consider, for example, irrigation frequency and timing, as well as irrigation methods (such as dripping, flooding). This can be achieved through coupling with more sophisticated land surface models, that is, Noah-MP (e.g., Zhang et al., 2017), or enhanced urban canopy model (e.g., Yang & Wang, 2015).

Even though the irrigated areas (including cropland and urban irrigation) constitute only around 9.1% of the entire inner domain (approximately 5,000 km<sup>2</sup>), the impacts can extend beyond the local scale through modifications of regional hydrometeorological fields and interactions between atmospheric forcing and complex terrain. Our results provide important implications for improved characterization of water and energy cycle in arid/semiarid southwestern United States under the context of climate change and intensified human activities. Future studies should extend the simulation to the entire North American Monsoon period for more robust characterizations of irrigation-induced changes in surface energy budget and water cycle.

### Acknowledgments

This research was financially supported by the National Key Research and Development Program of China (2018YFA0606002) and, the National Science Foundation grants (EAR-576 1632048, AGS-1522492, and CBET-1444758). L.Y. also acknowledges support from Strategic Priority Research Program of the Chinese Academy of Sciences (XDA 230402). The authors would also like to acknowledge high-performance computing support from Cheyenne provided by NCAR Computational and Information Systems Laboratory, sponsored by the National Science Foundation through projects UPRI0004 and UPRI0015. Observational data set are obtained through the Flood Control District of Maricopa (<http://alert.fcd.maricopa.gov/alert/Google/v3/wx.html> and <http://www.suominet.ucar.edu/data/staYrDay>) and the University of Wyoming radiosonde archive (<http://weather.uwyo.edu/upperair/sounding.html>).

### References

- Adams, D. K., & Comrie, A. C. (1997). The North American Monsoon. *Bulletin of the American Meteorological Society*, 78(10), 2197–2213. [https://doi.org/10.1175/1520-0477\(1997\)078<2197:TNAM>2.0.CO;2](https://doi.org/10.1175/1520-0477(1997)078<2197:TNAM>2.0.CO;2)
- Alter, R. E., Im, E.-S., & Eltahir, E. A. B. (2015). Rainfall consistently enhanced around the Gezira Scheme in East Africa due to irrigation. *Nature Geoscience*, 8(10), 763–767. <https://doi.org/10.1038/ngeo2514>
- Carleton, A. M. (1986). Synoptic-dynamic character of “bursts” and “breaks” in the South-West U.S. summer precipitation singularity. *Journal of Climatology*, 6(6), 605–623. <https://doi.org/10.1002/joc.3370060604>
- Chen, F., Kusaka, H., Bornstein, R., Ching, J., Grimmond, C. S. B., Grossman-Clarke, S., et al. (2011). The integrated WRF/urban modelling system: development, evaluation, and applications to urban environmental problems. *International Journal of Climatology*, 31(2), 273–288. <https://doi.org/10.1002/joc.2158>
- Chow, W. T. L., Brennan, D., & Brazel, A. J. (2012). Urban Heat Island research in Phoenix, Arizona: Theoretical contributions and policy applications. *Bulletin of the American Meteorological Society*, 93(4), 517–530. <https://doi.org/10.1175/bams-d-11-00011.1>
- Chow, W. T. L., Volo, T. J., Vivoni, E. R., Jenerette, G. D., & Ruddell, B. L. (2014). Seasonal dynamics of a suburban energy balance in Phoenix, Arizona. *International Journal of Climatology*, 34(15), 3863–3880. <https://doi.org/10.1002/joc.3947>
- DeAngelis, A., Dominguez, F., Fan, Y., Robock, A., Kustu, M. D., & Robinson, D. (2010). Evidence of enhanced precipitation due to irrigation over the Great Plains of the United States. *Journal of Geophysical Research*, 115, D15115. <https://doi.org/10.1029/2010JD013892>
- Diem, J. E. (2006). Anomalous monsoonal activity in central Arizona, USA. *Geophysical Research Letters*, 33, L16706. <https://doi.org/10.1029/2006GL027259>
- Diem, J. E., & Brown, D. P. (2003). Anthropogenic impacts on summer precipitation in central Arizona, U.S.A. *The Professional Geographer*, 55(3), 343–355. <https://doi.org/10.1111/0033-0124.5503011>
- D'Odorico, P., & Porporato, A. (2004). Preferential states in soil moisture and climate dynamics. *Proceedings of the National Academy of Sciences*, 101(24), 8848–8851. <https://doi.org/10.1073/pnas.0401428101>
- Douglas, M. W., Maddox, R. A., Howard, K., & Reyes, S. (1993). The Mexican Monsoon. *Journal of Climate*, 6(8), 1665–1677. [https://doi.org/10.1175/1520-0442\(1993\)006<1665:TMM>2.0.CO;2](https://doi.org/10.1175/1520-0442(1993)006<1665:TMM>2.0.CO;2)
- Eltahir, E. A. B. (1998). A soil moisture–rainfall feedback mechanism: 1. Theory and observations. *Water Resources Research*, 34(4), 765–776. <https://doi.org/10.1029/97WR03499>
- Findell, K. L., & Eltahir, E. A. B. (2003). Atmospheric controls on soil moisture–boundary layer interactions. Part I: framework development. *Journal of Hydrometeorology*, 4(3), 552–569. [https://doi.org/10.1175/1525-7541\(2003\)004<0552:acosml>2.0.co;2](https://doi.org/10.1175/1525-7541(2003)004<0552:acosml>2.0.co;2)
- Findell, K. L., Gentile, P., Lintner, B. R., & Kerr, C. (2011). Probability of afternoon precipitation in eastern United States and Mexico enhanced by high evaporation. *Nature Geoscience*, 4(7), 434–439. <https://doi.org/10.1038/ngeo1174>
- Fowler, M. D., Pritchard, M. S., & Kooperman, G. J. (2018). Assessing the impact of Indian irrigation on precipitation in the irrigation-enabled Community Earth System Model. *Journal of Hydrometeorology*, 19(2), 427–443. <https://doi.org/10.1175/JHM-D-17-0038.1>
- Georgescu, M., Mahalov, A., & Moustaki, M. (2012). Seasonal hydroclimatic impacts of Sun Corridor expansion. *Environmental Research Letters*, 7(3), 034026. <https://doi.org/10.1088/1748-9326/7/3/034026>
- Georgescu, M., Miguez-Macho, G., Steyaert, L. T., & Weaver, C. P. (2008). Sensitivity of summer climate to anthropogenic land-cover change over the Greater Phoenix, AZ, region. *Journal of Arid Environments*, 72(7), 1358–1373. <https://doi.org/10.1016/j.jaridenv.2008.01.004>
- Georgescu, M., Miguez-Macho, G., Steyaert, L. T., & Weaver, C. P. (2009a). Climatic effects of 30 years of landscape change over the Greater Phoenix, Arizona, region: 1. Surface energy budget changes. *Journal of Geophysical Research*, 114, D05110. <https://doi.org/10.1029/2008JD010745>
- Georgescu, M., Miguez-Macho, G., Steyaert, L. T., & Weaver, C. P. (2009b). Climatic effects of 30 years of landscape change over the Greater Phoenix, Arizona, region: 2. Dynamical and thermodynamical response. *Journal of Geophysical Research*, 114, D05111. <https://doi.org/10.1029/2008JD010762>
- Georgescu, M., Moustaki, M., Mahalov, A., & Dudhia, J. (2011). An alternative explanation of the semiarid urban area “oasis effect”. *Journal of Geophysical Research*, 116, D24113. <https://doi.org/10.1029/2011JD016720>
- Gober, P., Brazel, A., Quay, R., Myint, S., Grossman-Clarke, S., Miller, A., & Rossi, S. (2009). Using watered landscapes to manipulate urban heat island effects: How much water will it take to cool Phoenix? *Journal of the American Planning Association*, 76(1), 109–121. <https://doi.org/10.1080/01944360903433113>
- Gober, P., & Kirkwood, C. W. (2010). Vulnerability assessment of climate-induced water shortage in Phoenix. *Proceedings of the National Academy of Sciences*, 107(50), 21295–21299. <https://doi.org/10.1073/pnas.0911113107>
- Grossman-Clarke, S., Zehnder, J. A., Loridan, T., & Grimmond, C. S. B. (2010). Contribution of land use changes to near-surface air temperatures during recent summer extreme heat events in the Phoenix metropolitan area. *Journal of Applied Meteorology and Climatology*, 49(8), 1649–1664. <https://doi.org/10.1175/2010JAMC2362.1>
- Guillod, B. P., Orlowsky, B., Miralles, D. G., Teuling, A. J., & Seneviratne, S. I. (2015). Reconciling spatial and temporal soil moisture effects on afternoon rainfall. *Nature Communications*, 6(1), 6443. <https://doi.org/10.1038/ncomms7443>
- Hirt, P., Gustafson, A., & Larson, K. (2008). The mirage in the valley of the Sun. *Environmental History*, 13(3), 482–514. <https://doi.org/10.1093/envhis/13.3.482>
- Im, E. S., & Eltahir, E. A. B. (2014). Enhancement of rainfall and runoff upstream from irrigation location in a climate model of West Africa. *Water Resources Research*, 50, 8651–8674. <https://doi.org/10.1002/2014WR015592>

- Im, E. S., Marcella, M. P., & Eltahir, E. A. B. (2014). Impact of potential large-scale irrigation on the West African Monsoon and its dependence on location of irrigated area. *Journal of Climate*, 27(3), 994–1009. <https://doi.org/10.1175/jcli-d-13-00290.1>
- Kusaka, H., Kondo, H., Kikegawa, Y., & Kimura, F. (2001). A simple single-layer Urban Canopy Model for atmospheric models: Comparison with multi-layer and Slab Models. *Boundary-Layer Meteorology*, 101(3), 329–358. <https://doi.org/10.1023/A:1019207923078>
- Lemonsu, A., Viguié, V., Daniel, M., & Masson, V. (2015). Vulnerability to heat waves: Impact of urban expansion scenarios on urban heat island and heat stress in Paris (France). *Urban Climate*, 14, 586–605. <https://doi.org/10.1016/j.uclim.2015.10.007>
- Li, D., Bou-Zeid, E., Barlage, M., Chen, F., & Smith, J. A. (2013). Development and evaluation of a mosaic approach in the WRF-Noah framework. *Journal of Geophysical Research: Atmospheres*, 118, 11,918–11,935. <https://doi.org/10.1002/2013JD020657>
- Maddox, R. A., McCollum, D. M., & Howard, K. W. (1995). Large-scale patterns associated with severe summertime thunderstorms over central Arizona. *Weather and Forecasting*, 10(4), 763–778. [https://doi.org/10.1175/1520-0434\(1995\)010<0763:LSPAWS>2.0.CO;2](https://doi.org/10.1175/1520-0434(1995)010<0763:LSPAWS>2.0.CO;2)
- Mahalov, A., Li, J., & Hyde, P. (2016). Regional impacts of irrigation in Mexico and the southwestern United States on hydrometeorological fields in the North American Monsoon region. *Journal of Hydrometeorology*, 17(12), 2981–2995. <https://doi.org/10.1175/jhm-d-15-0223.1>
- Mazon, J. J., Castro, C. L., Adams, D. K., Chang, H.-I., Carrillo, C. M., & Brost, J. J. (2016). Objective climatological analysis of extreme weather events in Arizona during the North American Monsoon. *Journal of Applied Meteorology and Climatology*, 55(11), 2431–2450. <https://doi.org/10.1175/JAMC-D-16-0075.1>
- Mejia, J. F., Douglas, M. W., & Lamb, P. J. (2015). Observational investigation of relationships between moisture surges and mesoscale to large-scale convection during the North American monsoon. *International Journal of Climatology*, 36(6), 2555–2569. <https://doi.org/10.1002/joc.4512>
- Mitchell, V. G., Mein, R. G., & McMahon, T. A. (2001). Modelling the urban water cycle. *Environmental Modelling & Software*, 16(7), 615–629. [https://doi.org/10.1016/S1364-8152\(01\)00029-9](https://doi.org/10.1016/S1364-8152(01)00029-9)
- Oke, T. R. (1979). Advectively-assisted evapotranspiration from irrigated urban vegetation. *Boundary-Layer Meteorology*, 17(2), 167–173. <https://doi.org/10.1007/bf00117976>
- Oke, T. R. (2006). Initial guidance to obtain representative meteorological observations at urban sites. IOM Report No. 81. WMO/TD-No.1250. <http://www.wmo.int/pages/prog/www/IMOP/publications/IOM81/IOM-81-UrbanMetObs.pdf>
- Richter, B. (2013). Cities of the future: Where will the water come from? *American Water Works Association*, 105(9), 22–24. <https://doi.org/10.5942/jawwa.2013.105.0138>
- Salamanca, F., Zhang, Y., Barlage, M., Chen, F., Mahalov, A., & Miao, S. (2018). Evaluation of the WRF-Urban modeling system coupled to Noah and Noah-MP land surface models over a semiarid urban environment. *Journal of Geophysical Research: Atmospheres*, 123, 2387–2408. <https://doi.org/10.1002/2018JD028377>
- Seastrand, S., Serra, Y., Castro, C., & Ritchie, E. (2014). The dominant synoptic-scale modes of North American monsoon precipitation. *International Journal of Climatology*, 35(8), 2019–2032. <https://doi.org/10.1002/joc.4104>
- Skamarock, W. C., Klemp, J. B., Dudhia, J., Gill, D. O., Barker, M., Duda, K. G., et al. (2008). A description of the Advanced Research WRF version 3, Rep., 1–113 pp.
- Song, J., Wang, Z.-H., & Wang, C. (2018). The regional impact of urban heat mitigation strategies on planetary boundary layer dynamics over a semiarid city. *Journal of Geophysical Research: Atmospheres*, 123, 6410–6422. <https://doi.org/10.1029/2018JD028302>
- Taylor, C. M., de Jeu, R. A. M., Guichard, F., Harris, P. P., & Dorigo, W. A. (2012). Afternoon rain more likely over drier soils. *Nature*, 489(7416), 423–426. <https://doi.org/10.1038/nature11377>
- Templeton, N. P., Vivoni, E. R., Wang, Z.-H., & Schreiner-McGraw, A. P. (2018). Quantifying water and energy fluxes over different urban land covers in Phoenix, Arizona. *Journal of Geophysical Research: Atmospheres*, 123, 2111–2128. <https://doi.org/10.1002/2017JD027845>
- Vahmani, P., & Hogue, T. S. (2014). Incorporating an urban irrigation module into the Noah land surface model coupled with an Urban Canopy Model. *Journal of Hydrometeorology*, 15(4), 1440–1456. <https://doi.org/10.1175/jhm-d-13-0121.1>
- Vahmani, P., & Hogue, T. S. (2015). Urban irrigation effects on WRF-UCM summertime forecast skill over the Los Angeles metropolitan area. *Journal of Geophysical Research: Atmospheres*, 120, 9869–9881. <https://doi.org/10.1002/2015JD023239>
- Welty, J., & Zeng, X. (2018). Does soil moisture affect warm season precipitation over the Southern Great Plains? *Geophysical Research Letters*, 45, 7866–7873. <https://doi.org/10.1029/2018GL078598>
- Yang, J., & Wang, Z.-H. (2015). Optimizing urban irrigation schemes for the trade-off between energy and water consumption. *Energy and Buildings*, 107, 335–344. <https://doi.org/10.1016/j.enbuild.2015.08.045>
- Yang, J., Wang, Z. H., Chen, F., Miao, S., Tewari, M., Voogt, J. A., & Myint, S. (2015). Enhancing hydrologic modelling in the coupled Weather Research and Forecasting–Urban Modelling System. *Boundary-Layer Meteorology*, 155(1), 87–109. <https://doi.org/10.1007/s10546-014-9991-6>
- Yang, J., Wang, Z. H., Georgescu, M., Chen, F., & Tewari, M. (2016). Assessing the impact of enhanced hydrological processes on urban hydro meteorology with application to two cities in contrasting climates. *Journal of Hydrometeorology*, 17(4), 1031–1047. <https://doi.org/10.1175/JHM-D-15-0112.1>
- Yang, L., & Smith, J. (2018). Sensitivity of extreme rainfall to atmospheric moisture content in the arid/semiarid southwestern United States: Implications for probable maximum precipitation estimates. *Journal of Geophysical Research: Atmospheres*, 123, 1638–1656. <https://doi.org/10.1002/2017JD027850>
- Yang, L., Smith, J. A., Baeck, M. L., Morin, E., & Goodrich, D. C. (2017). Flash flooding in arid/semi-arid regions: Dissecting the hydro-meteorology and hydrology of the 19 August 2014 storm and flood hydroclimatolgy in Arizona. *Journal of Hydrometeorology*, 18(12), 3103–3123. <https://doi.org/10.1175/JHM-D-17-0089.1>
- Yang, Z., Dominguez, F., Gupta, H., Zeng, X., & Norman, L. (2015). Urban effects on regional climate: A case study in the Phoenix and Tucson “Sun Corridor”. *Earth Interactions*, 20(20), 1–25. <https://doi.org/10.1175/EI-D-15-0027.1>
- Zhang, X., Xiong, Z., & Tang, Q. (2017). Modeled effects of irrigation on surface climate in the Heihe River Basin, northwest China. *Journal of Geophysical Research: Atmospheres*, 122, 7881–7895. <https://doi.org/10.1002/2017JD026732>